Energy, Environmental, and Catalysis Applications

A Biocatalyst and Colorimetric/Fluorescent Dual Biosensors of H2O2 Constructed via Hemoglobin-Cu3(PO4)2 Organic/Inorganic Hybrid Nanoflowers

Jiaojiao Gao, Hui Liu, Lingyan Pang, Kai Guo, and Junqi Li

ACS Appl. Mater. Interfaces, **Just Accepted Manuscript** • DOI: 10.1021/acsami.8b10968 • Publication Date (Web): 14 Aug 2018

A Biocatalyst and Colorimetric/Fluorescent Dual Biosensors of H_2O_2 Constructed via Hemoglobin-$Cu_3(PO_4)_2$ Organic/Inorganic Hybrid Nanoflowers

Jiaojiao Gao, Hui Liu, Lingyan Pang*, Kai Guo, Junqi Li*

School of Materials Science and Engineering, Shaanxi University of Science and Technology, Xi'an 710021, P. R. China

ABSTRACT: In this paper, the 3-dimensional Hemoglobin (Hb)-$Cu_3(PO_4)_2$ organic/inorganic hybrid nanoflowers (Hb-$Cu_3(PO_4)_2$ HNFs) self-assembled by nanopetals were synthesized via a facile one-pot green synthetic method. The compositions and microstructure of the Hb-$Cu_3(PO_4)_2$ HNFs were well characterized with X-ray diffraction, scanning electron microscopy, transmission electron microscopy, X-ray photoelectron spectroscopy, Fourier transform infrared spectroscopy and UV-vis spectrometer, respectively. The as-prepared Hb-$Cu_3(PO_4)_2$ HNFs to be used as an biocatalyst to constructed colorimetric/fluorescent dual biosensors. The experimental results show that the colorimetric/fluorescent dual biosensors exhibited two linear responses in the range of 2-10 ppb and 20-100 ppb for H_2O_2. The colorimetric and fluorescent detection limits were 0.1 ppb and 0.01 ppb respectively. Compared with the free Hb, the biocatalytic activity of the Hb-$Cu_3(PO_4)_2$ HNFs can be improved for 3~4 times under the optimal conditions. The sensing performance of these Hb-$Cu_3(PO_4)_2$ HNFs based dual biosensors can be contributed that the active sites of Hb molecules were more exposed on the surface of the $Cu_3(PO_4)_2$ nanopetals. Secondly, the unique nanopetals assembled hybrid flower-like structure was favorable to contact of the detected substance with the biosensors. The dual biosensors were successfully applied for the determination

*Corresponding author. Tel: +86-29-86177018; Fax: +86-29-86177018.
Email address: liuhui@sust.edu.cn (Hui Liu)
*Corresponding author. Tel: +86-29-86177018; Fax: +86-29-86177018.
Email address: panglingyan@sust.edu.cn (Lingyan Pang)

of H_2O_2 in rainwater, tap water and waste water samples. These results show that the dual biosensors had potential application in the field of medical analysis, environmental monitoring and food engineering.

KEYWORDS: organic/inorganic hybrid nanoflower, hemoglobin, biosensor, fluorescent, colorimetric, H_2O_2

INTRODUCTION

Hydrogen peroxide (H_2O_2) is a common oxidizing agent and an essential intermediate or final product in food, biomedical, pharmaceutical, industrial and environmental and enzymatic reactions.[1-4] Researchers found that H_2O_2 is immediately dangerous to human health and life when its concentration exceeds to 75 ppm.[5] Thus, it is necessary and urgent to establish a quick and accurate method to monitoring the concentration of H_2O_2. In the fields of food, industry, environment, and clinical diagnosis, many methods have been explored for the detection of H_2O_2, such as electrochemical,[3] bioelectrochemical,[6] liquid chromatography,[7] colorimetric,[8] fluorescence analytic methods,[9] etc. Among the above methods, fluorescent and colorimetric analytic methods are broadly used for detection of H_2O_2 due to their peculiar advantages, such as low-cost, simplicity, high sensitivity and excellent practicability.[10-13] Especially, the fluorescent/colorimetric biosensors based on the biocatalytic activity of enzymes or other proteins are the main developing direction and research focus. So far several enzymes or other proteins, such as horseradish peroxidase (HRP), glucose oxidase (GOD), bovine serum albumin (BSA) and hemoglobin (Hb), are frequently used to construct of the fluorescent/colorimetric biosensors due to their high specificity and excellent catalytic activity.

Hb is a tetrameric heme protein consisting of aglobular protein and four iron-containing hemes.[14, 15] Heme is an important iron porphyrin compound, which is structurally similar to

peroxidases,[16, 17] and exhibits a mimetic peroxidase activity for the detection of H_2O_2. However, due to its complex structure, i.e., iron-containing heme active sites are deeply embedded in the peptide chains, Hb display a weak catalytic capacity compared with that of peroxidase although it has a preferable structural stability.[18] To solve the above problems, a few methods, such as chemical modified Hb,[19] Hb-polymer conjugates[20] and immobilization of Hb on nanomaterials,[21] have been reported to improve the exposure of hemoglobin active sites. Among these methods, immobilization of Hb on nanomaterials is a most commonly used method, which is favorable to exposes more highly accessible active sites and enhance the catalytic activity of Hb. A variety of nanomaterials have been developed as support matrix for immobilization of Hb, such as, SiO_2, carbon nanotube, CoO, Ag and TiO_2/graphene nanocomposite with different morphologies, etc.[22-26] Especially, flower-like nanostructure to be found have a better promoting effect for the enhancement of the biological activity of Hb molecules because this hierarchical structure show a large surface area, which is beneficial to expose more active sites on the surface of nanomaterials and contact of the detected substance with the Hb carrier.

In addition, the combination ways between nanomaterial and Hb exhibit an important influence on the biological activity of Hb. Traditionally, there are mainly four combination ways for the immobilization of proteins with nanomaterials: physical or chemical adsorption, covalent, entrapment and cross-linking.[27-30] Most of the immobilized proteins exhibit increasing stability, higher activity, and good repeatability. However, these conventional protein immobilization methods are very difficult to ensure the active sites of proteins while maintaining biological activity. Therefore, it is imperative to seek a new way for protein immobilization with high activity. Recently, Zare and co-workers[31] discovered that the flower-like organic-inorganic hybrid nanostructures composed of protein and copper (II) compound displayed much higher enzyme activity and stability

than free and conventional immobilized enzymes, which provided a novel enzyme immobilization approach that could greatly enhance the activity and stability of the enzyme.

Herein, we report the synthesis of a Hemoglobin (Hb)-$Cu_3(PO_4)_2$ organic/inorganic hybrid nanoflowers (Hb-$Cu_3(PO_4)_2$ HNFs) self-assembled by nanopetals through facile water-bath synthesis strategy. In this mild and green synthetic process, no toxic elements are involved. The flower-like structure make Hb-$Cu_3(PO_4)_2$ HNFs as a biocatalyst for H_2O_2 decomposition has many advantages as follows: Firstly, the active sites of Hb molecules are more exposed on the surface of Hb-$Cu_3(PO_4)_2$ HNF due to its special organic-inorganic hybrid structure. Meanwhile, the Hb-$Cu_3(PO_4)_2$ HNFs can be easily separated from the reaction system and reused several times. Secondly, $Cu_3(PO_4)_2$ nanopetals with excellent biocompatibility can provide a protective microenvironment for the Hb to retain their bioactivity and stability. Thirdly, the unique nanopetals assembled hybrid flower-like structure is favorable to contact of the detected substance with the biosensors. As shown in Scheme 1, Hb-$Cu_3(PO_4)_2$ HNFs can effectively accelerate the decomposition of H_2O_2 to hydroxyl radical (•OH) which can oxidize excess I^- to form I_3^- and then it combines with Rhodamine 6G (Rh6G) to form $(Rh6G\sim I_3)_n$ association particles. The $(Rh6G\sim I_3)_n$ association particle gives strong resonance scattering effect, fluorescence quenching, and hypochromatic color effect. Therefore, in the present report, a novel colorimetric/fluorescent dual biosensors of Hb-$Cu_3(PO_4)_2$ HNFs-based multi-substance biocatalytic system have been proposed and the proposed method has potential applications in the detection of H_2O_2 in rainwater, tap water and waste water.

EXPERIMENTAL SECTION

Materials and Aparatus. Hemoglobin (Hb, from bovine blood) was purchased from Sigma-Aldrich. Rhodamine 6G (Rh6G) was supplied by Shanghai Reagent Factory (China).

$CuSO_4 \cdot 5H_2O$, KI, H_2O_2 (30% w/v), $NaH_2PO_4 \cdot 2H_2O$, $Na_2HPO_4 \cdot 12H_2O$), CH_3COONa and CH_3COOH were obtained from Sinopharm Chemical Reagent Co., Ltd., China. All the reagents used were of analytical grade and ultrapure water (18.2 MΩ, Millipore, USA) was used for all experiments. The X-ray diffraction (Rigaku XRD, D/max2200, Japan, Cu Kα 0.154 nm) was used to analyze the crystal structures of Hb-$Cu_3(PO_4)_2$ HNFs. The microstructure and morphology of the Hb-$Cu_3(PO_4)_2$ HNFs were investigated by field-emission scanning electron microscope (FE-SEM, Hitachi S-4800 & Hiroba EDX electron microscopy) and transmission electronic microscopy (TEM, FEI Tecnai F20). The morphological changes were determined using environmental scanning electron microscopy (ESEM, FEI Q45). Surface electronic structure was analyzed by X-ray photoelectron spectroscopy (XPS, ESCALAB 250Xi). The decomposition process of the Hb molecule during heat treatment was characterized by the thermogravimetric-differential scanning calorimetry (TG-DSC, Netzsch Corporation STA409PC). Fourier-transform infrared (FTIR) spectra were recorded from sample powder palletized with KBr (sample ratio, 1.5 to 100 mg) on a Bruker TENSOR27. Ultraviolet-visible (UV-vis) absorption spectra were obtained using an Agilent Cary 5000 spectrophotometer. The fluorescence spectra emission spectra of the system were measured using an EDINBURGH FS5.

Synthesis of Hb-$Cu_3(PO_4)_2$ HNFs. In a typical experiment, an aqueous solution of $CuSO_4$ (120 mM, 60 μL) was added into 9 mL of phosphate buffered saline (PBS) solution (0.1 M, pH 7.4) containing different concentrations of Hb (0.05 mg/mL, 0.1 mg/mL and 0.5 mg/mL, labeled as HNFs-1, HNFs-2 and HNFs-3), followed by incubation at 25 °C for 3 day. After incubation, turquoise precipitates were collected by centrifugation (3500 rpm for 5 min) and the precipitate was washed with ultrapure water and stored in ultrapure water at 4 °C. Furthermore, to probe the growth mechanism of Hb-$Cu_3(PO_4)_2$ HNFs, the samples were prepared with different incubation times (1,

24, 48 and 72 h).

Detection of H_2O_2. The different concentrations of H_2O_2 solutions were prepared in water and the feasibility investigation of H_2O_2 sensing was carried out in HAc-NaAc buffer solution + Rh6G + KI + Hb-$Cu_3(PO_4)_2$ HNFs system. The detailed procedure was as follows: Firstly, 0.5 mL Rh6G (1.0×10^{-4} M), 0.3 mL HAc-NaAc buffer solution (0.1 M, pH 4.7), 0.7 mL KI aqueous solution (0.03 M), Hb (0.2 mL 1.0×10^{-5} M) or Hb-$Cu_3(PO_4)_2$ HNFs (0.2 mL 3.225 mg/mL), and equal volumes of different concentrations of H_2O_2 (5 μL, 0~1 ppm) were added into the centrifuge tube (10 mL), diluted to 5 mL with ultrapure water and shaked adequately. Subsequently, the reaction solution was centrifuged at 3500 rpm for 6 min to remove the Hb-$Cu_3(PO_4)_2$ HNFs. Finally, the colorimetric response (λ_{ab}=527 nm) as well as fluorescence response (λ_{em}=557 nm)of the supernatant was recorded by using the UV-Vis spectroscopy and fluorescent spectrometer, respectively.

Detecting H_2O_2 in Real Samples. The rainwater, tap water and waste water were collected without any treatment and stored at room temperature prior to analysis. The spiked samples were prepared by the addition of standard H_2O_2 in rainwater, tap water or waste water. The analysis process was similar to the sensing procedure, as described in Section 2.3.

RESULTS AND DISCUSSION

Chemical and Physical Structure of the Prepared Hb-$Cu_3(PO_4)_2$ HNF. To analyses the chemical and physical structure of the Hb-$Cu_3(PO_4)_2$ HNFs, XRD, SEM, TEM, EDX and XPS experiments have been conducted. The inset of Figure S1 shows the photo images of pure $Cu_3(PO_4)_2$ (top) and Hb-$Cu_3(PO_4)_2$ HNFs (down). On the macro point of view, the pure $Cu_3(PO_4)_2$ sample present a blue colour while the Hb-$Cu_3(PO_4)_2$ HNF is blue-green. This is mainly due to the fact that the Hb as an organic component in Hb-$Cu_3(PO_4)_2$ HNFs is red colour. Figure S1 present the XRD patterns of the Hb-$Cu_3(PO_4)_2$ HNFs (red curve) and pure $Cu_3(PO_4)_2$ (black curve). All

diffraction peaks in the XRD patters of both samples are match well with the JCPDS X-ray powder diffraction file of No. 22-0548 belong to $Cu_3(PO_4)_2 \cdot 3H_2O$). Compared with the pure $Cu_3(PO_4)_2 \cdot 3H_2O$ nanosheets, the relative intensities of all diffraction peaks of the Hb-$Cu_3(PO_4)_2$ HNFs is decreased. The reason is that the introduction of Hb reduced the crystallinity of the $Cu_3(PO_4)_2$ the relative intensities of all diffraction peaks of the Hb-$Cu_3(PO_4)_2$ HNFs.

To further confirm the composition and chemical configuration of the obtained Hb-$Cu_3(PO_4)_2$ HNFs, XPS analysis was carried out. Figure 1a shows the survey spectrum of the prepared Hb-$Cu_3(PO_4)_2$ HNFs. Besides the Cu 2p and P 2p signals belong to $Cu_3(PO_4)_2$ were observed, clear N 1s signal derived from hemoglobin molecules were also obtained. As for the signal of C 1s, it may be contributed to both of the hemoglobin molecules and detection environment. For the Cu 2p XPS spectrum (Figure 1b), the peaks corresponding to Cu $2p_{1/2}$ and Cu $2p_{3/2}$ were observed at 954.94 eV and 935.0 eV, respectively.[32] Compared with that of the pure $Cu_3(PO_4)_2 \cdot 3H_2O$ nanosheets counterparts (Figure S2), in which the Cu $2p_{1/2}$ and Cu $2p_{3/2}$ were located at the binding energies of 954.78 eV and 934.79 eV, respectively, the Cu $2p_{1/2}$ and Cu $2p_{3/2}$ peaks for Hb-$Cu_3(PO_4)_2$ HNFs shifted towards higher binding energy regions by amounts of 0.16 eV and 0.21 eV. This may be contributed that the Cu-N and Cu-O bonds are formed between Cu^{2+} and Hb molecules. Figure 1c shows the Fe 2p XPS spectrum, it can be found that the peaks Fe $2p_{3/2}$ and Fe $2p_{1/2}$ of Fe (III) were located at 711.33 eV and 721.46 eV, respectively. And the satellite peak founded at 716.54 eV indicates the presence of Fe (II) on the surface of the HNFs.[33, 34] Similarly, the Fe 2p of the pure Hb molecular was also analyzed by XPS (Figure S3). Notably, the peaks corresponded to Fe 2p were not found, indicating more active centers can be exposed in the organic-inorganic hybrid structure. The N 1s spectra of Hb-$Cu_3(PO_4)_2$ HNFs can be separated into C-N / N-H (399.62 eV) and N-C=O (400.0 eV) (Figure 1d) belong to Hb molecular.[35] The C1s XPS

spectrum of Hb-$Cu_3(PO_4)_2$ HNF was decomposed into four components, assigned to C-C/C-H (284.6 eV), C-S/C-N (286.1 eV), amide (287.7 eV) and carboxyl (289.7 eV) groups of the Hb molecules (Figure 1e).[36, 37] The XPS analysis was also found the binding energies of P 2p at 131.15 eV corresponded to characteristic of PO_4^{3-} (Figure 1f).[38]

Morphology of the Prepared Hb-$Cu_3(PO_4)_2$ HNF. Morphology of the Hb-$Cu_3(PO_4)_2$ HNF was exposed by SEM and TEM measurement. The SEM images of Hb-$Cu_3(PO_4)_2$ HNFs (Figure 2a and b) shows that the as-prepared sample display a regularly flower-like structure assembled by a great deal of interlaced nanopetals with the thickness of about 20~25 nm, and the average diameter of these hybrid nanoflower with good monodispersity were determined to be 10~15 μm. As shown in Figure 2c, the low-resolution TEM image of the partial nanoflower further confirmed the 3-D hierarchical structure of the Hb-$Cu_3(PO_4)_2$ HNFs. The high-resolution TEM image of the nanopetal was illustrated in Figure 2d. The spacing between adjacent lattice planes is 0.212 nm, corresponding to the diffraction peak at $2\theta = 41.988$. The actual area (BET) of Hb-$Cu_3(PO_4)_2$ HNF is 15.01 m^2/g and it turned out that the hierarchical flower-like structure can effectively increase the specific surface area of the biocatalysts, which is beneficial to contact with substrates and improve their biocatalytic activity (Figure S4). The energy dispersive X-ray spectroscopy (EDX) was further confirmed that the Hb-$Cu_3(PO_4)_2$ HNFs are consisted of Cu, P, C, O, N, Ca and Cl elements (Figure S5). As for the Ca and Cl elements, it may be derived from PBS solution.

Growth mechanisms of the prepared Hb-$Cu_3(PO_4)_2$ HNF. To monitoring the growth process of Hb-$Cu_3(PO_4)_2$ HNFs, time-depend ESEM, UV-vis and FT-IR experiments have been applied to analyses the as-prepared samples after the different growth stages. It is worth noting that in order to avoiding the destroy of the Hb molecular structure on the surface of the sample, the ESEM measurement was used to observe the growth process of Hb-$Cu_3(PO_4)_2$ HNFs. Before the detection,

the as-prepared Hb-$Cu_3(PO_4)_2$ HNFs were dispersed in an aqueous solution and maintained at a constant temperature of 20 °C. As shown in Figure 3a, a large numbers of chain-like complexes are observed after 1 h of incubation. The quaternary structure of Hb changed when Cu^{2+} is added into PBS containing Hb at pH 7.4. Subsequently, the four subunits dissociated from each other and then they can stretch into loose peptide chains.[39] It is known that the pI point of Hb is 6.7, which is lower than the pH value of the incubation system.[40] Therefore, the protein molecules were negatively charged and can form complexes with Cu^{2+} through coordination interactions of $-COO^-$ and amide groups in the Hb backbone.[41] Thus these chains are Cu^{2+}/Hb complexes and provided the growth sites for nucleation of the primary crystals. With the increasing of incubation time (24 h), some of curly petal-like nanosheets are appeared in Figure 3b. The growth of copper phosphate crystals were controlled by the kinetically under the induction of protein molecules and then the petals was generated. Additionally, it can also be found that the growth and self-assembly of petals were carried out at the same time. The self-assembled petals had further grown up after 48 h of incubation (Figure 3c). At the final stage, nanopetals were continuously grown up and assembled to form a three dimensional hierarchical flower-like structure when the incubation time reached 72 h (Figure 3d). The growth rate of the each part of reaction system is different due to the influence of the experimental operation. Therefore, there are some Hb-$Cu_3(PO_4)_2$ HNFs appearing in each time period. With the increasing of the incubation time (From 1 h to 24 h, 48 h and 72 h, respectively), the sizes of Hb-$Cu_3(PO_4)_2$ HNFs are 6.7 μm, 8 μm, 10.7 μm and 13.3 μm, respectively. This result show that the formation of the petals and the self-assembly of the Hb-$Cu_3(PO_4)_2$ HNFs were carried out at the same time. The nucleation of the copper phosphate crystals in protein molecules and then grew in different directions under the induction process of proteins. This special organic-inorganic hybrid structure enables Hb-$Cu_3(PO_4)_2$ HNFs to have the biological activity of the organic

components and the stability of the inorganic components, and can be easily separated from the reaction system. What's more, the conformational changes also expose more active centers on surface, which effectively increasing the peroxidase-like catalytic activity of Hb.

To verify the formation of the Hb-$Cu_3(PO_4)_2$ HNFs, pure Hb (curve a), $Cu_3(PO_4)_2 \cdot 3H_2O$ (curve f) and the Hb-$Cu_3(PO_4)_2$ HNFs (curve b, c, d and e) with different incubation time were analyzed by FT-IR spectroscopy (Figure S6). In the FT-IR spectra of pure Hb (curve a), typical absorption band of amide I was observed at 1652 cm^{-1}, which is attributed to C=O stretching vibration of peptide linkages in the backbone of protein.[42, 43] The absorption band at 1531 cm^{-1} is caused by the combination of N-H bending/C-N stretching (amide II) and -COO^- asymmetric stretching.[42-44] And the 1393 cm^{-1} band has been associated with the -COO^- symmetric stretching.[44, 45] As for the pure $Cu_3(PO_4)_2 \cdot 3H_2O$ (curve f), the absorption bands belong to phosphate groups were located at 1152 cm^{-1} (stretching vibration of P=O bond), 1049 cm^{-1} (asymmetrical stretching of P-O bond), 989 cm^{-1} (stretching vibration of P-O bond), 624 cm^{-1} (bending vibration of P-O bond) and 553 cm^{-1} (in-plane bending vibration phosphate ion).[46, 47] Compared with that of pure Hb and $Cu_3(PO_4)_2 \cdot 3H_2O$, the FT-IR spectra of Hb-$Cu_3(PO_4)_2$ HNFs prepared by different incubation time(Curve b, c, d and e) possess all the characteristic absorption bands of above mentioned. This proved that the prepared Hb-$Cu_3(PO_4)_2$ HNFs were composed of Hb and $Cu_3(PO_4)_2 \cdot 3H_2O$. And the presence of amide I and amide II also indicated that Hb retained the essential features of its native secondary structure in Hb-$Cu_3(PO_4)_2$ HNFs.[48] In addition, it is also found that the absorption bands of amide I (1659 cm^{-1}), amide II/-COO^- asymmetric stretching (1537 cm^{-1}) and -COO^- symmetric stretching (1401 cm^{-1}) of Hb-$Cu_3(PO_4)_2$ HNFs had a blue shift in the curve e. The blue shift of the three characteristic absorption bands of the Hb revealed that the coordination interaction between Cu^{2+} and the amide groups and -COO^- of Hb backbones.[41, 45] It is worth noting that a weak

absorption band at 520 cm^{-1} was also found in curve b, c, d and e, which can be attributed to the stretching vibration of Cu-O bond.[49] This further confirmed that a complex was formed between Cu^{2+} and protein molecules, and verified the previous conjecture. Moreover, it can be found that the intensities belong to the characteristic absorption bands of amide group, phosphate group and Cu-O bonds were progressively increased with the increasing of incubation time. The result indicated that the Cu^{2+}/Hb complexes were gradually increasing, and with continuous growth of the $Cu_3(PO_4)_2$ crystals, the amount of the immobilized enzyme was also significantly increased.

In order to further prove the immobilization effect of the Hb-$Cu_3(PO_4)_2$ HNFs ,UV-vis spectroscopy has been conducted on the supernatant from the Hb-$Cu_3(PO_4)_2$ HNFs suspension with different incubation time *(*1, 24, 48, and 72 h). Figure S7 show the Soret absorption band of heme was located at 405 nm, which was close to the pure Hb (401 nm). The Soret absorption band of heme proved existence on the conformational integrity of the Hb.[42, 50] With the increasing of incubation time, the concentrations of the Hb in the supernatant decreased immediately. Notably, the Soret absorption intensity of Hb display a dramatic reduction for the first 24 h particularly, and after 48 h incubation, the intensity of Hb have a little change with the increasing of incubation time, which indicating that most of the Hb molecular was consumed to form the Hb/Cu^{2+} complexes in the first 24 h.

Comprehensive analysis of time-depend ESEM, FT-IR and UV-Vis, the growth mechanisms of the Hb-$Cu_3(PO_4)_2$ HNFs can be conclude as follows: (□) early nucleation and formation of Cu^{2+}/Hb complexes, (□) growth of nanopetals, and (□) complete formation of three dimensional flower-like structures (as illustrated in Figure 3e).

Apart from the effect of incubation time, the concentration of Hb also plays important roles in the formation of Hb-$Cu_3(PO_4)_2$ HNFs. Figure S8 showed the SEM images of Hb-$Cu_3(PO_4)_2$ HNFs

prepared with different Hb concentrations. With the increasing of the Hb concentrations, the quantity of nucleation sites increased, leading to a more compact structure, while the size of HNFs was reduced. Correspondingly, the weight percentage of Hb in the Hb-$Cu_3(PO_4)_2$ HNF was determined by thermogravi-metric (TG) analysis. Figure S9 displayed the TG analysis spectrum of the Hb-$Cu_3(PO_4)_2$ HNFs (HNFs-1: 0.1 mg/mL) and the weight percentage of Hb was about 20.1%. It was shown that the weight percentage of Hb in the HNFs gradually increased from 0 to 23.76% with the increasing of Hb concentration (which increased from 0 to 0.5 mg/mL) (Table S1). The encapsulation efficiency (defined as the ratio of the amount of immobilized enzyme to the total amount of enzyme employed) of Hb in Hb-$Cu_3(PO_4)_2$ HNF was determined by UV-vis spectroscopy method. With the increasing of Hb concentration (which increased from 0.05 to 0.5 mg/mL), the encapsulation efficiency decreased from 87.75 to 58.47% (Table S2). According to the results of tests, the concentration of Hb has impact on the morphology and catalysis of Hb-$Cu_3(PO_4)_2$ HNF. The lower the Hb concentration, more large the size of nanopetals, and then the three-dimensional structure is not easily to be maintained. At the Hb concentration of 0.5 mg/mL, the Hb-$Cu_3(PO_4)_2$ HNF exhibits an overdense flower-like structure as well as the highest Hb conten. But the active site of Hb is again blocked in the inorganic microspheres due to the overdense structure.

Therefore, in all the following experiments, the optimum synthesis conditions of the Hb-$Cu_3(PO_4)_2$ HNF are as follows: reaction temperature 25□, pH 7.4, incubation time 72 h and the concentration of Hb is 0.1 mg/m.

Catalytic mechanism and Kinetics of Hb-$Cu_3(PO_4)_2$ HNF. The catalytic activity of Hb-$Cu_3(PO_4)_2$ HNF was confirmed in the multi-substance biocatalytic system (HAc-NaAc + Rh6G + KI + H_2O_2). As illustrated in Scheme 1, H_2O_2 can be catalyzed to product hydroxyl radical (·OH) by Hb immobilized in Hb-$Cu_3(PO_4)_2$ HNFs, and then I^- can be oxidized to I_2 by ·OH.[51] Of excessive

I^- can be combined with I_2 to form I_3^-, and I_3^- reacts with Rh6G to form hydrophobic Rh6G~I_3 ion-association complexes. Finally, these hydrophobic complexes can easily aggregate into a larger $(Rh6G\sim I_3)_n$ association particles. The reaction mechanism of system is described as follows:

$$Hb(Fe^{□}) + H_2O_2 + H^+ \rightarrow Hb(Fe^{□}) + \cdot OH + H_2O \quad (1)$$

$$\cdot OH + I^- \rightarrow I_2 \quad (2)$$

$$I_2 + I^- \rightarrow I_3^- \quad (3)$$

$$I_3^- + R□6G^+ \rightarrow R□6G\sim I_3 \quad (4)$$

$$n\ R□6G\sim I_3 \rightarrow (R□6G\sim I_3)_n \quad (5)$$

In multi-substance biocatalytic system, Rh6G is selected as the indicator due to its excellent absorption and fluorescent properties.[52, 53] As shown in Figure S10, Rh6G exhibits a strongest absorption peak at 527 nm and a strongest fluorescence peak at 557 nm under excitation at 500 nm. The formation of $(Rh6G\sim I_3)_n$ associative nanoparticles can result in decreasing of the absorbance and the fluorescent intensity of the system. According to the Beer-Lambert law:[54]

$$A = KbC \quad (6)$$

where A is the absorbance value, K is the molar absorption coefficient, b is the thickness of the solution, and C represents the substrate concentration. The absorbance is proportional to the concentration of the absorbing substrate when the thickness of the solution is constant. From Equation (1)-(5), the relationship between the H_2O_2 concentration C_1 and the Rh6G concentration C_2 is $C_2 = C_0 - C_1/2$ (C_0 is the initial concentration of Rh6G in system). Then, the equation of A = kbc is written as:

$$A = Kb(C_0 - \frac{C_1}{2}) \quad (7)$$

Equation (7) indicates that the A is inverse proportional to the concentration of the H_2O_2 while other conditions are kept constant. So a catalytic kinetics determination methods of Hb-$Cu_3(PO_4)_2$

HNFs were investigated, meanwhile, a method for for detection of H_2O_2 concentration was constructed based on hypochromatic color effect and fluorescence quenching of Rh6G.

The time-dependent absorbance changes (ΔA) of Rh6G at the three systems (without Hb, free Hb and Hb-$Cu_3(PO_4)_2$ HNFs) are showed in Figure 4. Here, the initial concentration of Rh6G was 1.0×10^{-5} M in all the systems. Without the addition of free or immobilized Hb, ΔA_{527} increased slowly and reached the reaction platform over 82 min. When the free Hb was added into the system, the reaction time was about 62 min and it decreased about a quarter of the previous. This indicates that the Hb had a catalytic activity for the system. Remarkably, the reaction time of system reduced to only 15 min under the addition of Hb-$Cu_3(PO_4)_2$ HNFs, which indicate that the immobilization of Hb on the Hb-$Cu_3(PO_4)_2$ HNFs can immensely enhance the catalytic activity of Hb. The Inset of Figure 4 show that the approximate linear relationship between -ln I_{sub} (I_{sub} is the value obtained by subtracting the real-time ΔA from the saturated one) and t (the reaction time), indicating the pseudo-first-order kinetics of the system.[55] According to the linear relationship, the average reaction rate of constants (k) is 3.048×10^{-1} min^{-1}, 5.827×10^{-2} min^{-1} and 3.087×10^{-2} min^{-1} under the addition of the HNFs, free Hb and without Hb, respectively. This enhancement in the catalytic activity of the Hb-$Cu_3(PO_4)_2$ HNFs compared to free Hb can be ascribed to Hb stabilization by flower-like structures featuring large surface areas and extensive confinement, which promotes the accessibility of the substrate to the active sites of Hb.

Colorimetic and Fluorescent Detection of H_2O_2. Based on the biocatalytic properties mentioned above, the Hb-$Cu_3(PO_4)_2$ HNFs could be used as a biocatalyst to build the colorimetic/fluorescent dual sensors for H_2O_2. Figure 5 shows the UV absorbance and fluorescence emission intensity of different biocatalytic reaction systems. Strong absorbance and fluorescence emission intensity were observed at 527 nm and 557 nm in system $1^{\#}$, which accord with the

characteristic of Rh6G. For the addition of KI (system $2^{\#}$), free Hb (system $3^{\#}$) or H_2O_2 (system $4^{\#}$) alone into the system $1^{\#}$, there are little effect on the absorbance and fluorescence emission intensity of Rh6G. The addition of Hb-$Cu_3(PO_4)_2$ HNFs (system $5^{\#}$) decreased the absorbance and fluorescence emission intensity of system $1^{\#}$ slightly. This change can be mainly attributed that the Hb-$Cu_3(PO_4)_2$ HNFs had a few amount of adsorption for Rh6G, resulting the concentration reduction of Rh6G in the reaction system. The simultaneous addition of KI and H_2O_2 (system $6^{\#}$) to the system $1^{\#}$ caused a decrease of the absorbance and fluorescence emission intensity of Rh6G, which reveal that reactions can occur under this experiment conditions. Free Hb and Hb-$Cu_3(PO_4)_2$ HNFs as catalyst were respectively added into system $6^{\#}$, causing different degrees of decline of the absorbance and fluorescence emission intensity in system $7^{\#}$ and system $8^{\#}$. System $8^{\#}$ has the most to the decline of the absorbance and fluorescence emission intensity, followed by system $7^{\#}$ and system $6^{\#}$. Such results are mainly ascribed to the excellent catalytic performance of Hb-$Cu_3(PO_4)_2$ HNFs. In addition, the influence of different H_2O_2 concentration on the biocatalytic reaction efficiency is further explored (Figure S11). With the increasing of H_2O_2 concentration increasing from 2 ppb to 1000 ppb, the time, which the absorbance (λ=527 nm) of system reached the platform, is shorted immediately to 15min from the previous 40 min. This experimental result indicates that system $8^{\#}$ can be used for the detection of H_2O_2.

The biosensor performance for the detection of H_2O_2 of the HAc-NaAc + Rh6G + KI + HNFs system was also investigated through colorimetic/fluorescent dual methods. The color variations of the biocatalytic system were observed and the results were shown in the inset of Figure 6 A. With the increasing of H_2O_2 concentration, the color of the solution gradually changed from pink to colorless. Subsequently, the absorbance of Rh6G at 527 nm of system with the concentration of H_2O_2 was further tested by UV-vis spectrophotometer, as shown in the Figure 6A. An obvious

decrease in the absorption peak at 527 nm was clearly observed with increasing of H_2O_2 concentration from 0 to 1000 ppb. Figure 6B demonstrates the variation curve between the absorbance and H_2O_2 concentration. Two linear ranges are found between the absorbance and H_2O_2 concentration in the range of 2-10 ppb (R^2=0.9900) and 20-100 ppb (R^2=0.9928), the limitation of detection (LOD) of H_2O_2 detection limit was ~ 0.1 ppb (Inset in Fig. 6B a and b).

Similarly, the biocatalytic system also could be used to detect the concentration of H_2O_2 through fluorescent method. Upon increasing the concentration of H_2O_2, the fluorescence intensity of the solution changed from strong to weak under 365 nm UV light (inset in Figure 7A). Figure 7A shows the normalized emission spectra of biocatalytic reaction systems in the presence of H_2O_2 at different concentrations (0-1000 ppb). The emission peak of system was gradually quenched with the increasing of the H_2O_2concentration (0-1000 ppb). This was mainly due to the fact that the formation of Rh6G~I_3 association particles caused the fluorescent quenching. Figure 7B showed the changes of emission intensities versus H_2O_2 concentration. Two good linear relationships could be observed with the H_2O_2 concentration ranging from 2 ppb-10 ppb (R^2=0.9913) and 20-100 ppb (R^2=0.9969), respectively (Inset in Figure 7B a and b). The corresponding detection limitation was calculated to be 0.01 ppb (if the detection limitation is defined as the H_2O_2 concentration at which fluorescent intensity decrease could be observed).

Compared with the analytic methods for H_2O_2 detection in recent studies, the present biosensor shows an extremely low detection limit and a broader linear range. (Table S3).[56-59] The excellent sensing performance of dual biosensors can be ascribed to the high catalytic activity of Hb-$Cu_3(PO_4)_2$ HNFs and the stability of system, which resulting in the gradual changes of color and fluorescence quenching. Besides, the colorimetric/fluorescent dual biosensors can greatly reduce the error caused by the change of environmental conditions by output of two related measurement

results, and ensure the reliability of the measurement results.

Selectivity and Interference Immunity of the Sensors. High selectivity and interference immunity were important indicators to evaluate the performance of the biosensor. Here, seventeen possible coexisting substances in the system for fluorescent response are measured. Table S4 shows the relative error (%) obtained in the presence of each interfering substance (at a coexisting substance/H_2O_2 ratio of 100:1), compared to the response for H_2O_2 alone. No remarkable changes in the fluorescent intensity were observed in the presence of ascorbic acid, glucose, uric acid, dopamine, citric acid, a number of common metal ions (Fe^{3+}, Fe^{2+}, Na^{2+}, Mg^{2+}, Ca^{2+}, Mn^{2+}, Ni^{2+}, and Co^{2+}), and some anions/cations (NH_4^+, Cl^-, SO_4^{2-} and NO_3^-). The maximum relative error was -7.78 %, which indicated that the fluorescent method possessed an excellent selectivity and interference immunity towards H_2O_2 detection. Similarly, the interference immunity of colorimetric method was detected under the same condition, the maximum relative error was 12.04 %, as shown in table S5. Hence, the system showed a good selectivity and interference immunity for H_2O_2 for colorimetric/fluorescent methods constructed in this study.

Real Sample Analysis. To investigate the practical application of the dual biosensors, the detection of H_2O_2 in rainwater, tap water and waste water samples was carried out. The samples (rainwater, tap water and waste water) were used in the detection without any pretreatment. Rainwater samples (containing Rh6G, KI, HAc-NaAc buffer solution) exhibited an obvious color change from pink to colorless with the increasing of concentration of H_2O_2 (Photo images inset of Figure 8a). As shown in Fig. 8a, an obvious reducing in the absorption peak at 527 nm was clearly observed with the increasing of the H_2O_2 concentration. And the curve of UV absorbance versus H_2O_2 concentration was obtained (Inset on Figure 8a). In addition, the practicability of the fluorescent method for detection of H_2O_2 in rainwater is also verified. Upon the addition of different

concentration of H_2O_2 (1, 10, 100 and 1000 ppb) in rainwater, a gradual fluorescence change from strong yellow color to colorless is observed in rainwater system (Photo inset on Figure 8b). As shown in Figure 8b, with the increasing of H_2O_2 concentration, the characteristic emission peak intensity of Rh6G gradually decreased. And the curve of fluorescence emission intensity versus H_2O_2 concentration is shown in the inset of Figure 8b. The absorbance and fluorescence emission intensity of the spiked rainwater samples depended on the concentration of H_2O_2, suggesting the feasibility of the proposed method.

In addition, the H_2O_2concentration in the tap water and waste water sample had been also tested by colorimetric and fluorescent method. Figure S12 show the experimental results of tap water and waste water samples, containing different concentrations of H_2O_2, detected by colorimetric and fluorescent method, respectively. As shown in Table S6, all the experimental data are based on three duplicated measurement, the three real samples were analyzed by using colorimetric method. The recovery is between 102.82 % and 112.36 % and the relative standard deviation values varied from 0.04% to 0.72 %. Besides, the recovery was between 88.95 % and 112.35 % and the relative standard deviation values varied from 1.25 % to 6.01 % through fluorescent method (Table S7). The results demonstrated that the dual colorimetric/fluorescent biosensors based on HAc-NaAc + Rh6G + KI + HNF system possessed considerable potential for the practical detection of H_2O_2 in real water samples.

Stability and Reusability of Hb-$Cu_3(PO_4)_2$ HNFs. To substantiate the Hb-$Cu_3(PO_4)_2$ HNF had excellent performance as a biocatalyst, their reusability and stability were investigated through two methods. The reusability of the Hb-$Cu_3(PO_4)_2$ HNF was researched by determining the relative activities against over the course of eight rounds of reaction (Figure S13a). The HNF lost 19.35 % of its catalytic activity over the course of eight rounds of reaction by using fluorescent method.

Meanwhile, the catalytic activity of the HNF lost 15.62 % by using UV method (Figure S13b). The stability of the Hb-$Cu_3(PO_4)_2$ HNF was further compared with that of free Hb by fluorescent and UV methods. As for the fluorescent method (Figure S13c), the Hb-$Cu_3(PO_4)_2$ HNFs maintained more than 89.7 % of its catalytic activity after one month of storage in PBS solution at room temperature, while the free Hb only retained about 43.61 % of its initial activity. As for the UV method (Figure S13d), the HNF maintained 88.6 % of its catalytic activity and the free Hb retained about 47.97 %. It was worth pointing out that all the tests did not result in any obvious morphological change for the HNFs (Figure S14). Testing results demonstrated that the Hb-$Cu_3(PO_4)_2$ HNFs exhibited fantastic reusability and stability in the chemical environment of the biocatalytic reaction.

CONCLUSIONS

In summary, flower-like Hb-$Cu_3(PO_4)_2$ HNFs have been synthesized through a simple and green one-pot method, and subsequently it can serve as a biocatalyst to fabricate a colorimetric/fluorescent dual biosensors for the detection of H_2O_2. As one hybrid material, the Hb-$Cu_3(PO_4)_2$ HNFs possesses a excellent stability and exhibits enhanced catalytic activity in comparison with the free Hb. The unique nanopetals assembled hybrid flower-like structure is favorable to contact of the detected substance with the biosensors. According to the reasons above, the prepared biosensors display a wide linear range of 2-10, 20-100 ppb, a low detection limit of 0.01 ppb (fluorescent method) and 0.1 ppb (colorimetric method) for H_2O_2. The successful applications in real sample analysis suggest that the proposed biosensors have great potential in environmental monitoring.

ASSOCIATED CONTENT

Supporting Information

The Supporting Information is available free of charge on the ACS Publications website.

Detailed datas for the Hb-$Cu_3(PO_4)_2$ HNFs characterization, activity assays, reusability and stability studies, real sample analysis, including Figures S1-14 and Tables S1-7 (PDF)

AUTHOR INFORMATION

Corresponding Author

*E-mail: liuhui@sust.edu.cn (Hui Liu)

*E-mail: panglingyan@sust.edu.cn (Lingyan Pang)

Notes

The authors declare no competing financial interest.

ACKNOWLEDGMENTS

We acknowledge financially support from the National Science Foundation of China (51272147), the Natural Science Foundation of Shaanxi Province (2015JM5208), the Foundation for Young Scholars of Shaanxi University of Science &Technology (No. 2017BJ06), the Natural Science Foundation of Shaanxi Province（No.2018JQ2069) and the Graduate Innovation Found of Shaanxi University of Science & Technology.

REFERENCES

1. Muralikrishna, S.; Cheunkar, S.; Lertanantawong, B.; Ramakrishnappa, T.; Nagaraju, D. H.; Surareungchai, W.; Balakrishna, R. G.; Reddy, K. R. Graphene Oxide-Cu(II) Composite Electrode for Non-Enzymatic Determination of Hydrogen Peroxide. *Electroanal. Chem.* **2016**, *776*, 59-65.

2. Sun, L.; Ding, Y.; Jiang, Y.; Liu, Q. Montmorillonite-Loaded Ceria Nanocomposites with Superior Peroxidase-Like Activity for Rapid Colorimetric Detection of H_2O_2. *Sens. Actuators, B* **2017**, *239*, 848-856.

3. Xu, F.; Deng, M.; Li, G.; Chen, S.; Wang, L. Electrochemical Behavior of Cuprous

Oxide-Reduced Graphene Oxide Nanocomposites and Their Application in Nonenzymatic Hydrogen Peroxide Sensing. *Electrochim. Acta* **2013**, *88*, 59-65.

4. Samuni, U. Novel Catalytic Antioxidative Activity of Nitroxide Radicals in the Heme/H_2O_2 System. *Biophys.* **2009**, *96*, 436a-436a.

5. Sun, J.; Li, C.; Qi, Y.; Guo, S.; Xue, L. Optimizing Colorimetric Assay Based on V_2O_5 Nanozymes for Sensitive Detection of H_2O_2 and Glucose. *Sensors* **2016**, *16*, 584.

6. Xu, S.; Bo, P.; Han, X. A Third-generation H_2O_2 Biosensor Based on Horseradish Peroxidase-Labeled Au Nanoparticles Self-assembled to Hollow Porous Polymeric Nanopheres. *Biosens. Bioelectron.* **2007**, *22*, 1807-1810.

7. Yue, H.; Bu, X.; Huang, M. H.; Young, J.; Raglione, T. Quantitative Determination of Trace Levels of Hydrogen Peroxide in Crospovidone and a Pharmaceutical Product Using High Performance Liquid Chromatography with Coulometric Detection. *Int. J. Pharm.* **2009**, *375*, 33-40.

8. Chen, S.; Hai, X.; Chen, X. W.; Wang, J. H. In Situ Growth of Silver Nanoparticles on Graphene Quantum Dots for Ultrasensitive Colorimetric Detection of H_2O_2 and Glucose. *Anal. Chem.* **2014**, *86*, 6689-6694.

9. Huan, Y. F.; Fei, Q.; Shan, H. Y.; Wang, B. J.; Xu, H.; Feng, G. D. A Novel Water-soluble Sulfonated Porphyrin Fluorescence Sensor for Sensitive Assays of H_2O_2 and Glucose. *Analyst* **2015**, *140*, 1655-1661.

10. Han, M.; Wang, L.; Li, S.; Bai, L.; Zhou, Y.; Sun, Y.; Huang, H.; Li, H.; Liu, Y.; Kang, Z. High-bright Fluorescent Carbon Dot as Versatile Sensing Platform. *Talanta* **2017**, *174*, 265-273.

11. Huang, J.; Li, T.; Liu, R.; Zhang, R.; Wang, Q.; Li, N.; Gu, Y.; Wang, P. Rational Designed Benzochalcone-Based Fluorescent Probe for Molecular Imaging of Hydrogen Peroxide in Live Cells and Tissues. *Sens. Actuators, B* **2017**, *248*, 257-264.

12. Liu, Q.; Chen, P.; Xu, Z.; Chen, M.; Ding, Y.; Yue, K.; Xu, J. A Facile Strategy to Prepare Porphyrin Functionalized ZnS Nanoparticles and Their Peroxidase-like Catalytic Activity for Colorimetric Sensor of Hydrogen Peroxide and Glucose. *Sens. Actuators, B* **2017**, *251*, 339-348.

13. Yin, Y.; Chen, L. G.; Qi, X.; Guo, L.; Lin, Z.; Cai, Z.; Yang, H. H. Protein-Metal Organic Framework Hybrid Composites with Intrinsic Peroxidase-like Activity as a Colorimetric Biosensing Platform. *Acs Appl Mater Interfaces* **2016***, 8(42)*, 29052-29061.

14. Cai, C.; Chen, J. Direct Electron Transfer and Bioelectrocatalysis of Hemoglobin at a Carbon Nanotube Electrode. *Anal. Biochem.* **2004**, *325*, 285-292.

15. Lu, C.; Shen, Q.; Zhao, X.; Zhu, J.; Guo, X.; Hou, W. Ag Nanoparticles Self-supported on $Ag_2V_4O_{11}$ Nanobelts: Novel Nanocomposite for Direct Electron Transfer of Hemoglobin and Detection of H_2O_2. *Sens. Actuators, B* **2010**, *150*, 200-205.

16. Mot, A. C.; Bischin, C.; Muresan, B.; Parvu, M.; Damian, G.; Vlase, L.; Silaghidumitrescu, R. Antioxidant Activity Evaluation by Physiologically Relevant Assays Based on Haemoglobin Peroxidase Activity and Cytochrome C-induced Oxidation of Liposomes. *Nat. Prod. Res.* **2016**, *30*, 1315-1319.

17. Souza, T. T. L.; Moraes, M. L.; Ferreira, M. Use of Hemoglobin as Alternative to Peroxidases in Cholesterol Amperometric Biosensors. *Sens. Actuators, B* **2013**, *178*, 101-106.

18. Sun, B.; Ni, X.; Cao, Y.; Cao, G. Electrochemical Sensor Based on Magnetic Molecularly Imprinted Nanoparticles Modified Magnetic Electrode for Determination of Hb. *Biosens. Bioelectron.* **2017**, *91*, 354-358.

19. Torres, E.; Vazquez-Duhalt, R. Chemical Modification of Hemoglobin Improves Biocatalytic Oxidation of PAHs. *Biochem. Biophys. Res. Commun.* **2000**, *273*, 820-823.

20. Thilakarathne, V.; Briand, V. A.; Zhou, Y.; Kasi, R. M.; Kumar, C. V. Protein Polymer

Conjugates: Improving the Stability of Hemoglobin with Poly(acrylic acid). *Langmuir* **2011**, *27*, 7663-7671.

21. Qi, H.; Zhang, C.; Li, X. Amperometric Third-generation Hydrogen Peroxide Biosensor Incorporating Multiwall Carbon Nanotubes and Hemoglobin. *Sens. Actuators, B* **2006**, *114*, 364-370.

22. Sun, J. Y.; Huang, K. J.; Zhao, S. F.; Fan, Y.; Wu, Z. W. Direct Electrochemistry and Electrocatalysis of Hemoglobin on Chitosan-room Temperature Ionic Liquid-$TiO_{(2)}$-graphene Nanocomposite Film Modified Electrode. *Bioelectrochemistry* **2011**, *82*, 125-130.

23. Yang, M.; Qu, F.; Li, Y.; He, Y.; Shen, G.; Yu, R. Direct Electrochemistry of Hemoglobin in Gold Nanowire Array. *Biosens. Bioelectron.* **2007**, *23*, 414-420.

24. Zhu, Z.; Li, X.; Zeng, Y.; Sun, W.; Zhu, W.; Huang, X. Application of Cobalt Oxide Nanoflower for Direct Electrochemistry and Electrocatalysis of Hemoglobin with Ionic Liquid as Enhancer. *J. Phys. Chem.* **2011**, *115*, 12547-12553.

25. Zhang, R.; Wang, X.; Shiu, K. K. Accelerated Direct Electrochemistry of Hemoglobin Based on Hemoglobin-Carbon Nanotube (Hb-CNT) Assembly. *J. Colloid Interface Sci.* **2007**, *316*, 517-522.

26. He, P.; Hu, N.; Rusling, J. F. Driving Forces for Layer-by-layer Self-assembly of Films of SiO_2 Nanoparticles and Heme Proteins. *Langmuir* **2004**, *20*, 722-729.

27. Baptistapires, L.; Pérezlópez, B.; Mayorgamartinez, C. C.; Moralesnarváez, E.; Domingo, N.; Esplandiu, M. J.; Alzina, F.; Sotomayortorres, C. M.; Merkoçi, A. Electrocatalytic Tuning of Biosensing Response Through Electrostatic or Hydrophobic Enzyme-graphene Oxide Interactions. *Biosens. Bioelectron.* **2014**, *61*, 655-662.

28. Mateo, C.; Grazu, V.; Palomo, J. M.; Lopezgallego, F.; Fernandezlafuente, R.; Guisan, J. M. Immobilization of Enzymes on Heterofunctional Epoxy Supports. *Nat. Protoc.* **2007**, *2*, 1022-1033.

29. Tielmann, P.; Kierkels, H.; Zonta, A.; Ilie, A.; Reetz, M. T. Increasing the Activity and Enantioselectivity of Lipases by Sol-gel Immobilization: Further Advancements of Practical Interest. *Nanoscale* **2014**, *6*, 6220-6228.

30. Li, Z.; Morel, M.; Rudiuk, S.; Baigl, D. Intramolecularly Protein□Crosslinked DNA Gels: New Biohybrid Nanomaterials with Controllable Size and Catalytic Activity. *Small* **2017**, *13(28)*,1700706.

31. Ge, J.; Lei, J.; Zare, R. N. Protein-Inorganic Hybrid Nanoflowers. *Nat. Nanotechnol.* **2012**, *7*, 428-432.

32. Yohai, L.; Schreiner, W. H.; Vázquez, M.; Valcarce, M. B. Phosphate Ions as Inhibiting Agents for Copper Corrosion in Chlorinated Tap Water. *Mater. Chem. Phys.* **2013**, *139*, 817-824.

33. Yu, C.; Zhou, X.; Gu, H. Immobilization, Direct Electrochemistry and Electrocatalysis of Hemoglobin on Colloidal Silver Nanoparticles-Chitosan Film. *Electrochim. Acta* **2010**, *55(28)*, 8738-8743.

34. Eerenstein, W.; Morrison, F. D.; Dho, J.; Blamire, M. G.; Scott, J. F.; Mathur, N. D. Comment on "Epitaxial $BiFeO_3$ Multiferroic Thin Film Heterostructures". *Science* **2005**, *307(5713)*, 1203; author reply 1203.

35. Li, S.; Xia, J.; Liu, C.; Zheng, Y.; Zeng, L.; Hu, J.; Li, Q. Direct Electrochemistry and Electrocatalysis of Hemoglobin on an Indium Tin Oxide Electrode Modified with Implanted Carboxy Ions. *Microchim. Acta* **2009**, *167*, 41-46.

36. Zhang, Z.; Zhang, Y.; Song, R.; Wang, M.; Yan, F.; He, L.; Feng, X.; Fang, S.; Zhao, J.; Zhang, H. Manganese(II) Phosphate Nanoflowers as Electrochemical Biosensors for the High-sensitivity Detection of Ractopamine. *Sens. Actuators, B* **2015**, *211*, 310-317.

37. Wang, J. Y.; Chou, T. C.; Chen, L. C.; Ho, K. C. Using Poly(3-aminophenylboronic acid) Thin

Film with Binding-Induced Ion Flux Blocking for Amperometric Detection of Hemoglobin A1c. *Biosens. Bioelectron.* **2015**, *63*, 317-324.

38. Lee, M. Y.; Ding, S. J.; Wu, C. C.; Peng, J.; Jiang, C. T.; Chou, C. C. Fabrication of Nanostructured Copper Phosphate Electrodes for the Detection of α-amino Acids. *Sens. Actuators, B* **2015**, *206*, 584-591.

39. Berg, J. M.; Tymoczko, J. L.; Stryer, L. Biochemistry. 5th Edition. *National Center for Biotechnology Informationõs Bookshelf* **2006**, 93-126.

40. Tadera, K.; Minami, Y.; Chohchi, M. Interaction between Acidic Polysaccharides and Proteins. *Biosci.Biotechnol.Biochem* **2003**, *67*, 1840-1843.

41. Bertrán, J.; L. Rodríguezsantiago, A.; Sodupe, M. The Different Nature of Bonding in Cu^{+}-Glycine and Cu^{2+}-Glycine. *J.phys.chem.b* **1999**, *103*, 2310-2317.

42. Sun, W.; Guo, Y.; Ju, X.; Zhang, Y.; Wang, X.; Sun, Z. Direct Electrochemistry of Hemoglobin on Graphene and Titanium Dioxide Nanorods Composite Modified Electrode and Its Electrocatalysis. *Biosens. Bioelectron.* **2013**, *42*, 207-213.

43. Ma, W.; Tian, D. Direct Electron Transfer and Electrocatalysis of Hemoglobin in ZnO Coated Multiwalled Carbon Nanotubes and Nafion Composite Matrix. *Bioelectrochemistry* **2010**, *78*, 106-112.

44. Wang, W. B.; Huang, D. J.; Kang, Y. R.; Wang, A. Q. One-step in Situ Fabrication of a Granular Semi-IPN Hydrogel Based on Chitosan and Gelatin for Fast and Efficient Adsorption of Cu^{2+} ion. *Colloids Surf. B* **2013**, *106*, 51-59.

45. Martínez, J. M. L.; Rodríguez-Castellón, E.; Sánchez, R. M. T.; Denaday, L. R.; Buldain, G. Y.; Orto, V. C. D. XPS Studies on the Cu(I,II)-Polyampholyte Heterogeneous Catalyst: An Insight Into Its Structure and Mechanism. *J. Mol. Catal. A: Chem.* **2011**, *339*, 43-51.

46. Demadis, K. D.; Papadaki, M.; Aranda, M. A. G.; Cabeza, A.; Oliverapastor, P.; Sanakis, Y. Stepwise Topotactic Transformations (1D to 3D) in Copper Carboxyphosphonate Materials: Structural Correlations. *Cryst. Growth Des.* **2015**, *10*, 357-364.

47. Weber, M.; Nart, F. C. On the Adsorption of Ionic Phosphate Species on Au(111)-an in Situ FTIR Study. *Electrochim. Acta* **1996**, *41*, 653-659.

48. Lu, X.; Zhang, H.; Ni, Y.; Zhang, Q.; Chen, J. Porous Nanosheet-Based ZnO Microspheres for the Construction of Direct Electrochemical Biosensors. *Biosens. Bioelectron.* **2008**, *24*, 93-98.

49. Dar, M. A.; Kim, Y. S.; Kim, W. B.; Sohn, J. M.; Shin, H. S. Structural and Magnetic Properties of CuO Nanoneedles Synthesized by Hydrothermal Method. *Appl. Surf. Sci.* **2008**, *254*, 7477-7481.

50. Dong, S.; Zhang, P.; Liu, H.; Li, N.; Huang, T. Direct Electrochemistry and Electrocatalysis of Hemoglobin in Composite Film Based on Ionic Liquid and NiO Microspheres with Different Morphologies. *Biosens. Bioelectron.* **2011**, *26*, 4082-4087.

51. Sadrzadeh, S. M.; Graf, E.; Panter, S. S.; Hallaway, P. E.; Eaton, J. W. Hemoglobin. A Biologic Fenton Reagent. *J. Biol. Chem.***1984**, *259*, 14354-14356.

52. Sánchezvalencia, J. R.; Blaszczyklezak, I.; Espinós, J. P.; Hamad, S.; Gonzálezelipe, A. R.; Barranco, A. Incorporation and Thermal Evolution of Rhodamine 6G Dye Molecules Adsorbed in Porous Columnar Optical SiO_2 Thin Films. *Langmuir* **2009**, *25*, 9140-9148.

53. Liang, A. H.; Jiang, Z. L.; Zhang, B. M.; Liu, Q. Y.; Lan, J.; Lu, X. New Resonance Scattering Spectral Method for the Determination of Trace Amounts of Iodate with Rhodamine 6G. *Anal. Chim. Acta* **2005**, *530*, 131-134.

54. Liang, Z. X.; Zhao, T. S.; Xu, C.; Xu, J. B. Microscopic Characterizations of Membrane Electrode Assemblies Prepared under Different Hot-pressing Conditions. *Electrochim. Acta* **2007**, *53*, 894-902.

55. Wang, L. B.; Wang, Y. C.; He, R.; Zhuang, A.; Wang, X.; Zeng, J.; Hou, J. G. A New Nanobiocatalytic System Based on Allosteric Effect with Dramatically Enhanced Enzymatic Performance. *J. Am. Chem. Soc.* **2013**, *135*, 1272-1275.

56. Wang, X.; Hu, J.; Zhang, G.; Liu, S. Highly Selective Fluorogenic Multianalyte Biosensors Constructed via Enzyme-catalyzed Coupling and Aggregation-Induced Emission. *J. Am. Chem. Soc.* **2014**, *136*, 9890-9893.

57. Li, Z.; Xiao, Y.; Yin, Y.; Hu, W.; Liu, W.; Yang, H. Facile Synthesis of Enzyme-Inorganic Hybrid Nanoflowers and Its Application as a Colorimetric Platform for Visual Detection of Hydrogen Peroxide and Phenol. *Acs Appl Mater. Interfaces* **2014**, *6*, 10775-10782.

58. Liu, H.; Guo, K.; Duan, C.; Dong, X.; Gao, J. Hollow TiO_2 Modified Reduced Graphene Oxide Microspheres Encapsulating Hemoglobin for a Mediator-free Biosensor. *Biosens. Bioelectron* **2017**, *87*, 473-479.

59. Song, M.; Wang, J.; Chen, B.; Wang, L. A Facile, Non-reactive Hydrogen Peroxide (H_2O_2) Detection Method Enabled by Ion Chromatography with UV Detector. *Anal. Chem.* **2017**, *89*, 11537-11544.

Figure Captions:

Scheme 1. Schematic illustration of multi-substance biocatalytic reaction systems for H_2O_2 detection based on the Hb-$Cu_3(PO_4)_2$ HNFs.

Figure 1. XPS spectra of Hb-$Cu_3(PO_4)_2$ HNFs (a) survey spectrum, (b) Cu 2p, (c) Fe 2p, (d) N 1s, (e) C 1s and (f) P 2p.

Figure 2. Representative (a-b) SEM and (c-d) TEM images of Hb-$Cu_3(PO_4)_2$ HNFs.

Figure 3. ESEM images of Hb-$Cu_3(PO_4)_2$ HNFs under different incubation time of (a) 1 h, (b) 24 h, (c) 48 h, (d) 72 h. (e) Schematic illustration of growth progresses of Hb-$Cu_3(PO_4)_2$ HNF.

Figure 4. Catalytic kinetics of three biocatalysts reaction systems; Inset: Plots of $-\ln I_{sub}$ vs time for three catalytic systems. Experimental conditions: room temperature, 1.0×10^{-5} M Rh6G, 4.2×10^{-3} M KI and 1 ppm H_2O_2 in HAc-NaAc buffer solution (0.1 M, pH 4.8) for each system.

Figure 5. (a) Fluorescence emission intensity (λ_{em}=557 nm) and (b) UV-vis absorbance (λ_{ab}=527 nm) of different biocatalytic reaction systems. Inset top: fluorescence photograph extinction at 365nm of different biocatalytic reaction systems. Inset down: photograph in sunlight of different biocatalytic reaction systems (The reaction was carried out at room temperature for 15 min in all cases, H_2O_2 = 1 ppm, $1^{\#}$. HAc-NaAc + Rh6G; $2^{\#}$. HAc-NaAc + Rh6G + KI; $3^{\#}$. HAc-NaAc + Rh6G + Hb; $4^{\#}$. HAc-NaAc + Rh6G + H_2O_2; $5^{\#}$. HAc-NaAc + Rh6G + HNF; $6^{\#}$. HAc-NaAc + Rh6G + KI + H_2O_2; $7^{\#}$. HAc-NaAc + Rh6G + KI + Hb + H_2O_2; $8^{\#}$. HAc-NaAc + Rh6G + KI + HNFs + H_2O_2).

Figure 6. (A) The UV-vis absorbance spectra of biocatalytic reaction system in the presence of H_2O_2 at different concentrations. Inset: colorimetric responses of the sensing system in the presence of different concentration of H_2O_2. (B) H_2O_2 concentration dependence of normalized absorbance at 527 nm. Inset: the linear calibration plot for H_2O_2 concentration (a) 0-10 ppb and (b) 10-100 ppb.

Figure 7. (A) Normalized emission spectra of biocatalytic reaction systems in the presence of H_2O_2 at different concentrations (0-1000 ppb). Inset: fluorescent responses of the sensing system in the presence of different concentration of H_2O_2. (B) H_2O_2 concentration dependence of normalized emission intensities at 557 nm. Inset: The linear calibration plot for H_2O_2 concentration (a) 0-10 ppb and (b) 10-100 ppb.

Figure 8. (a) UV-vis absorption spectra of the rainwater with different concentrations of H_2O_2; Photo inset: visual color change of the rainwater; Inset: plot of absorbance versus H_2O_2 concentrations and visual color change; (b) Fluorescence emission spectra of the rainwater with different concentrations of H_2O_2; Photo inset: visual fluorescence change of the rainwater; Inset: plot of emission intensities versus H_2O_2 concentration and fluorescence change.

Scheme 1

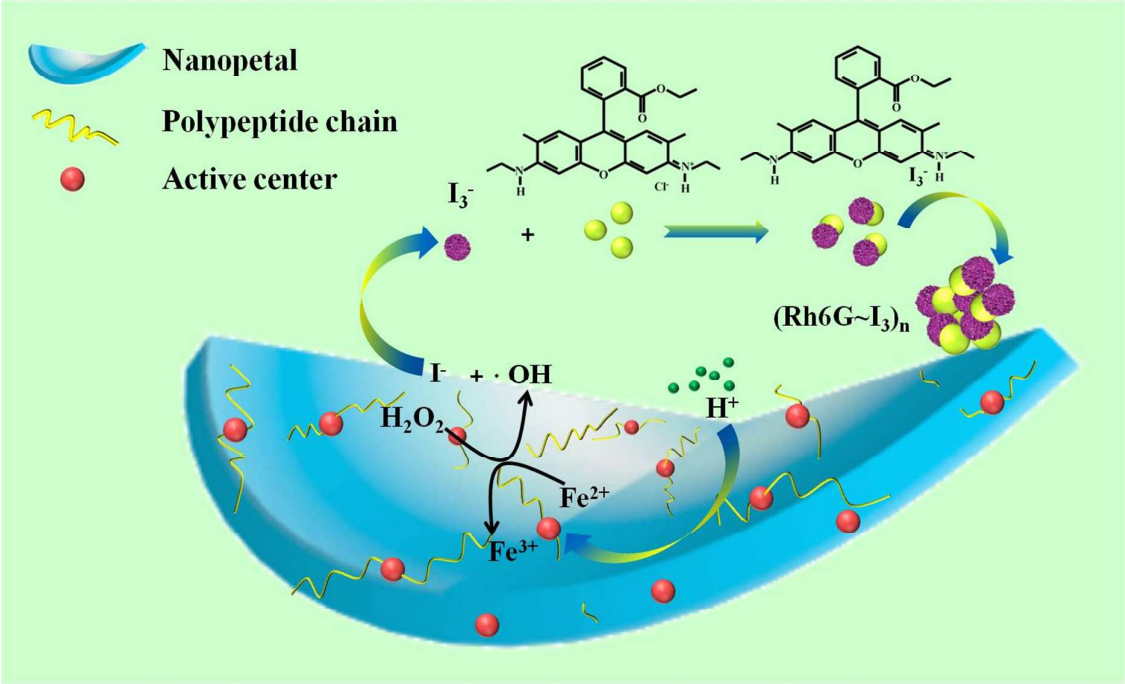
Nanopetal
Polypeptide chain
Active center
I_3^-
+
$(Rh6G\sim I_3)_n$
I^- + · OH
H_2O_2
H^+
Fe^{2+}
Fe^{3+}

Figure 1

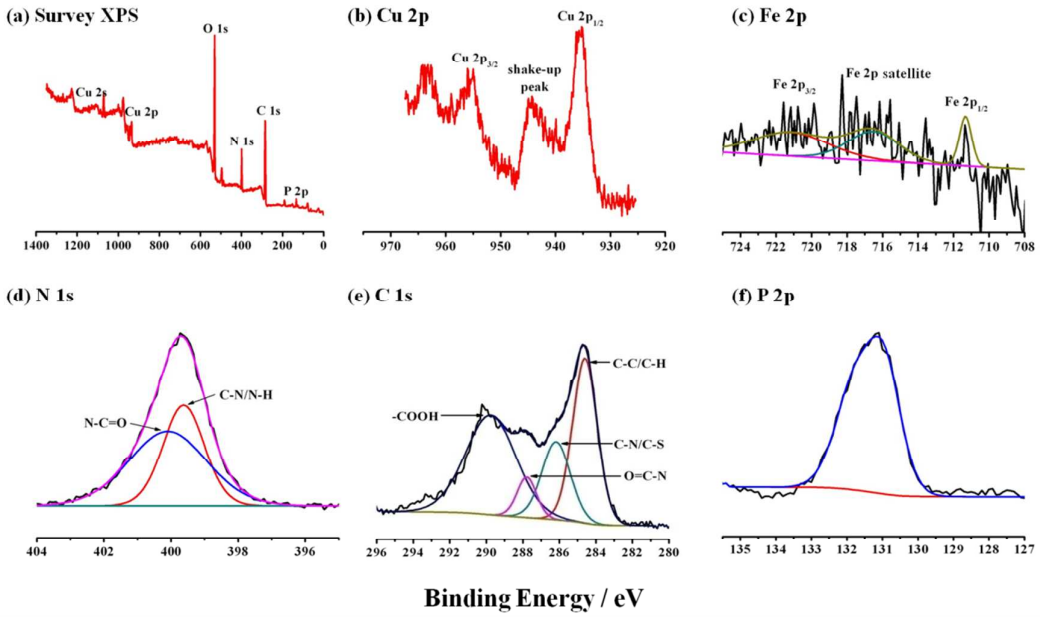
(a) Survey XPS
O 1s
Cu 2s
Cu 2p
C 1s
N 1s
P 2p
1400 1200 1000 800 600 400 200 0
(b) Cu 2p
Cu 2p1/2
Cu 2p3/2
shake-up peak
970 960 950 940 930 920
(c) Fe 2p
Fe 2p3/2
Fe 2p satellite
Fe 2p1/2
724 722 720 718 716 714 712 710 708
(d) N 1s
C-N/N-H
N-C=O
404 402 400 398 396
(e) C 1s
C-C/C-H
-COOH
C-N/C-S
O=C-N
296 294 292 290 288 286 284 282 280
(f) P 2p
135 134 133 132 131 130 129 128 127
Binding Energy / eV

Figure 2

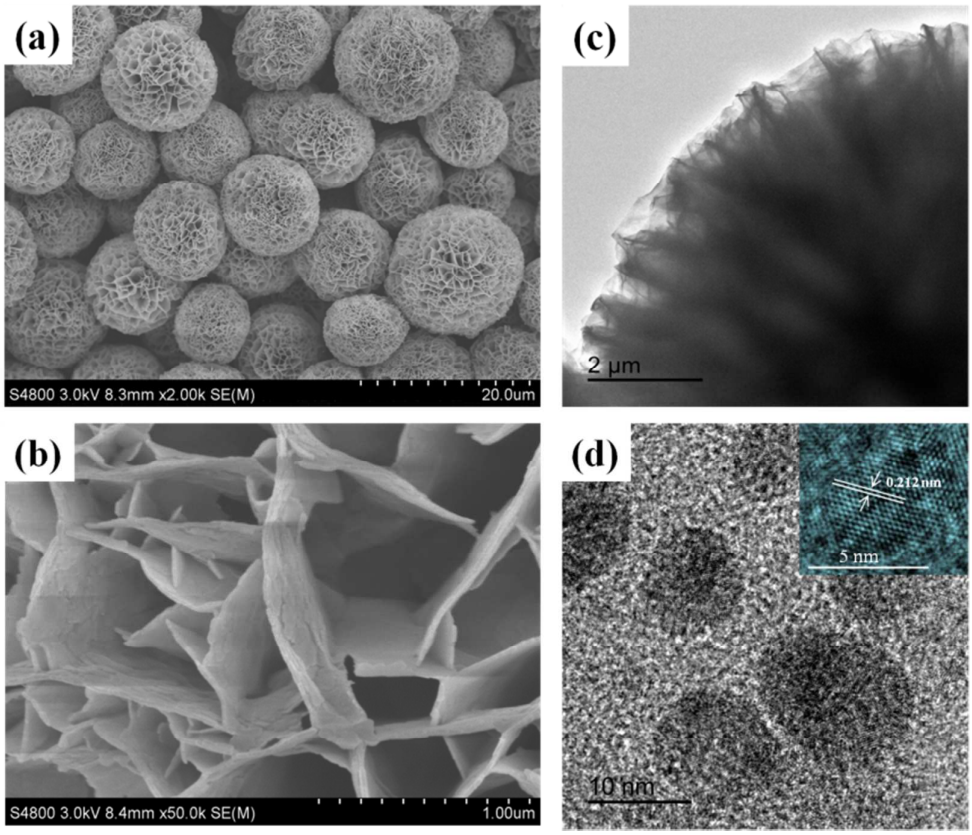
(a)
S4800 3.0kV 8.3mm x2.00k SE(M)
20.0um
(c)
2 μm
(b)
S4800 3.0kV 8.4mm x50.0k SE(M)
1.00um
(d)
0.212 nm
5 nm
10 nm

Figure 3

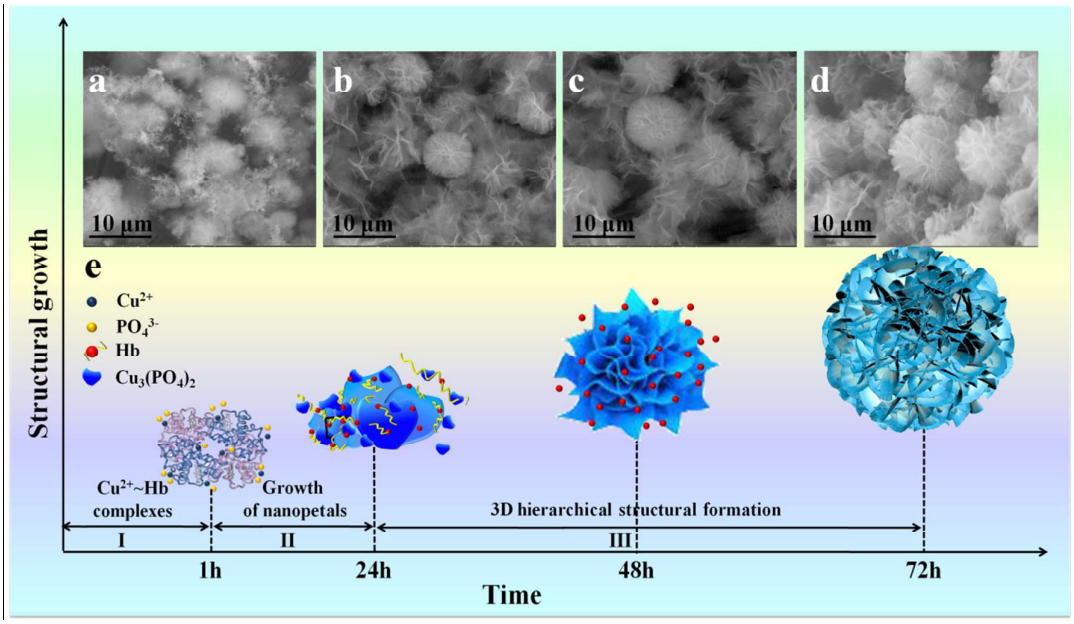
a
b
c
d
10 μm
10 μm
10 μm
10 μm
e
Cu2+
PO43-
Hb
Cu3(PO4)2
Structural growth
Cu2+~Hb complexes
Growth of nanopetals
3D hierarchical structural formation
I
II
III
1h
24h
48h
72h
Time

Figure 4

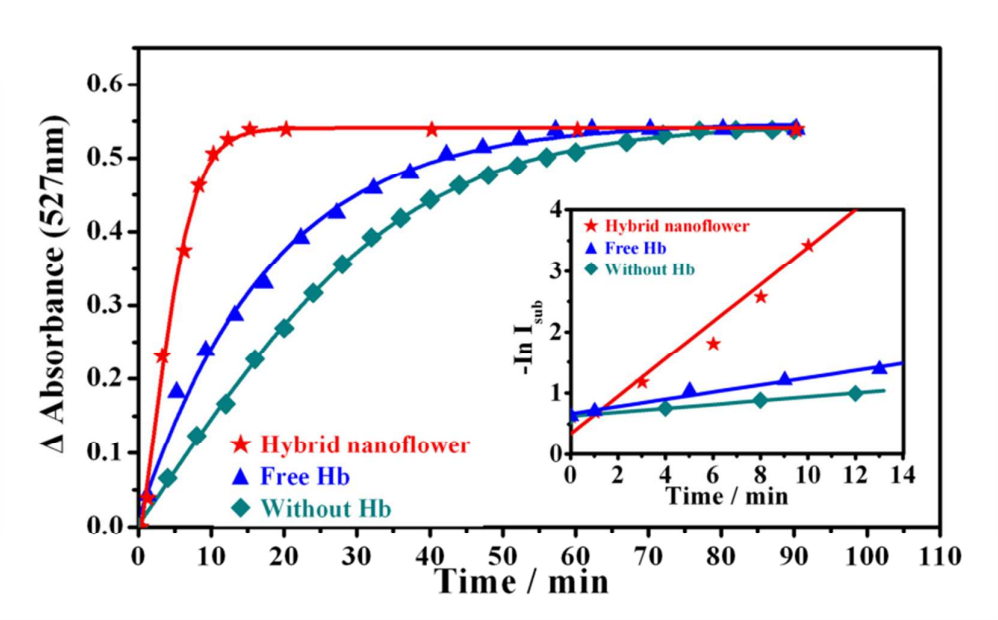
Δ Absorbance (527nm)
Time / min
Hybrid nanoflower
Free Hb
Without Hb
-ln I sub
Time / min
Hybrid nanoflower
Free Hb
Without Hb

Figure 5

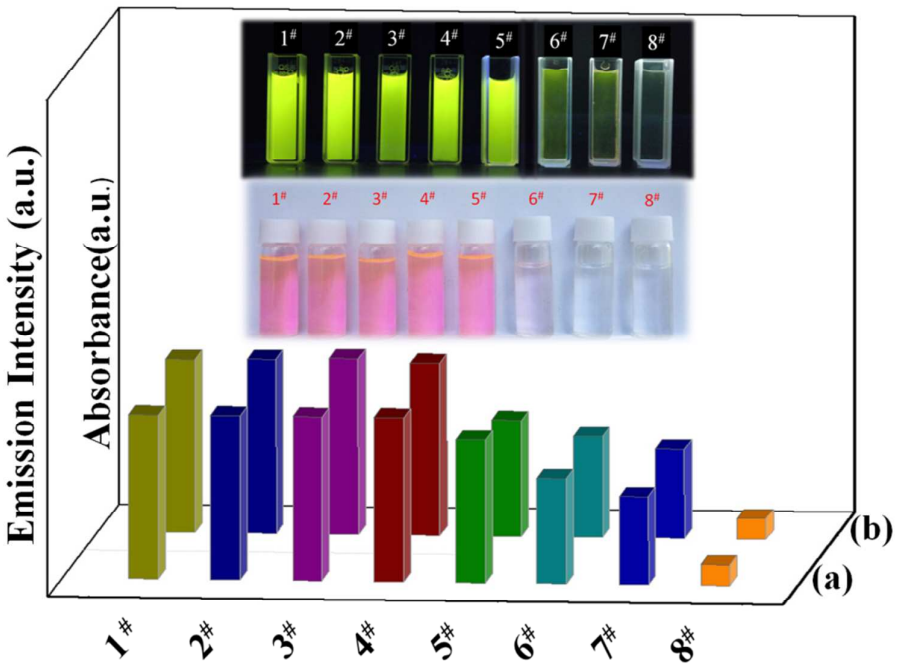
1# 2# 3# 4# 5# 6# 7# 8#
1# 2# 3# 4# 5# 6# 7# 8#
Emission Intensity (a.u.)
Absorbance(a.u.)
(b)
(a)
1# 2# 3# 4# 5# 6# 7# 8#

Figure 6

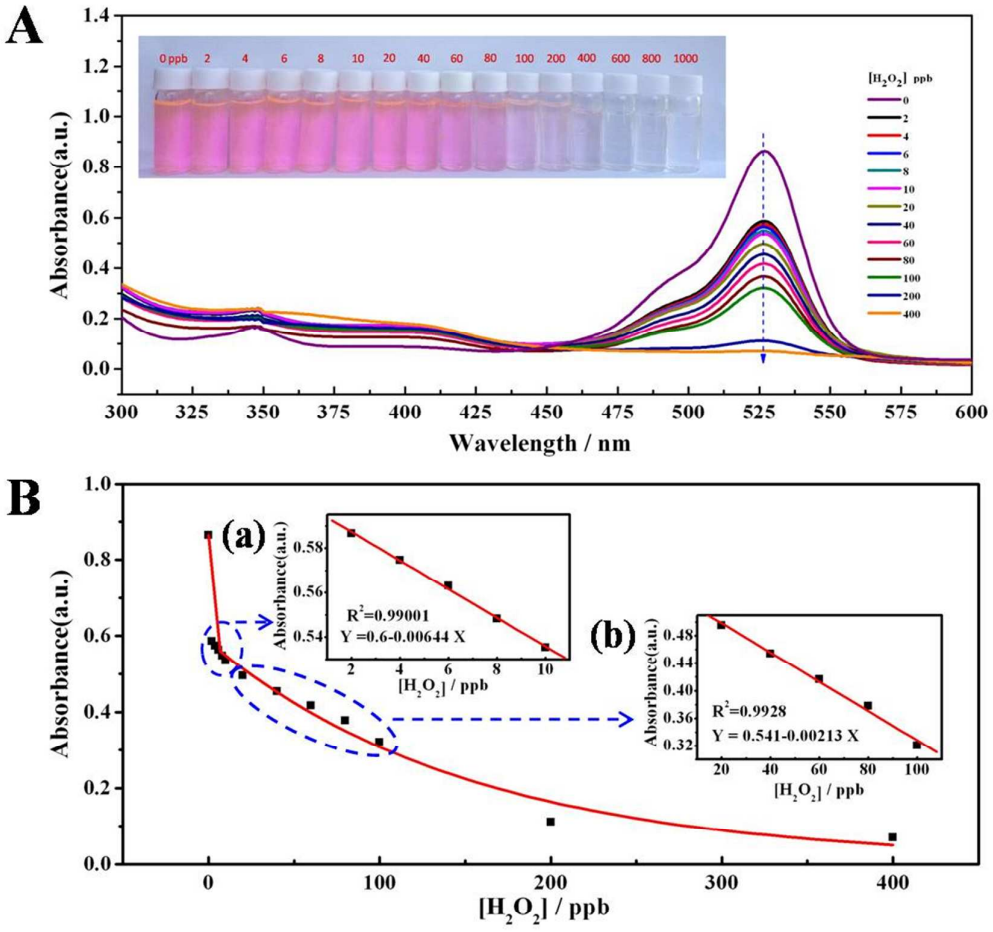
A
0 ppb 2 4 6 8 10 20 40 60 80 100 200 400 600 800 1000
[H2O2] ppb
0
2
4
6
8
10
20
40
60
80
100
200
400
Absorbance(a.u.)
Wavelength / nm
B
(a)
R2=0.99001
Y =0.6-0.00644 X
[H2O2] / ppb
(b)
R2=0.9928
Y = 0.541-0.00213 X
[H2O2] / ppb
Absorbance(a.u.)
[H2O2] / ppb

Figure 7

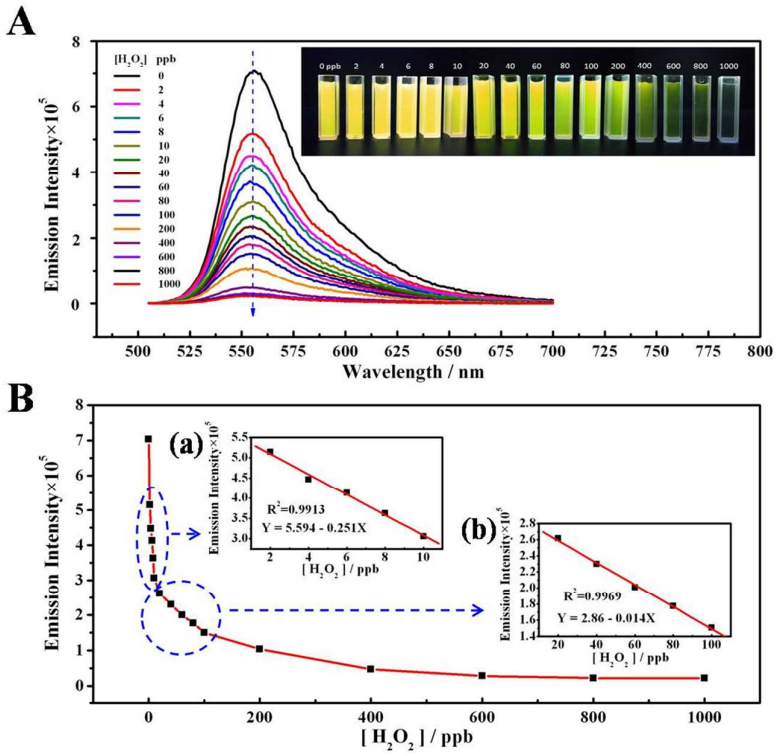
A
[H2O2] ppb
0
2
4
6
8
10
20
40
60
80
100
200
400
600
800
1000
Emission Intensity×10^5
Wavelength / nm
B
(a)
(b)
R²=0.9913
Y = 5.594 - 0.251X
R²=0.9969
Y = 2.86 - 0.014X
[H2O2] / ppb

Figure 8

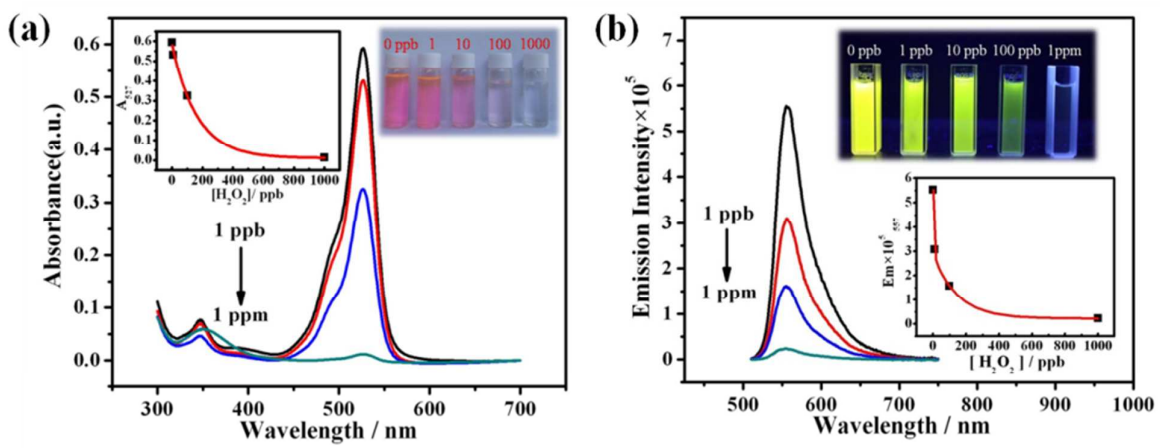
(a)
Absorbance(a.u.)
Wavelength / nm
1 ppb
1 ppm
0 ppb 1 10 100 1000
[H2O2]/ ppb
(b)
Emission Intensity×10^5
Wavelength / nm
1 ppb
1 ppm
0 ppb 1 ppb 10 ppb 100 ppb 1ppm
[H2O2] / ppb

TOC graphic

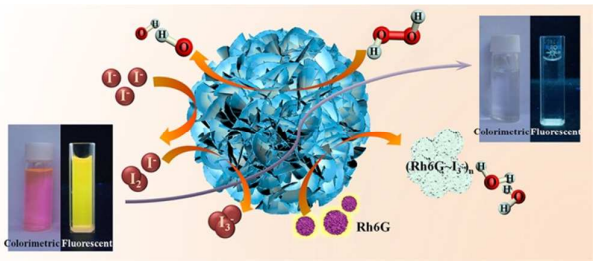
Colorimetric
Fluorescent
Rh6G
Colorimetric
Fluorescent